Journal of Nuclear Materials 385 (2009) 126–130

Contents lists available at ScienceDirect

Journal of Nuclear Materials

journal homepage: www.elsevier.com/locate/jnucmat

EXAFS study of the structural phase transition in the americium zirconate pyrochlore

P.M. Martin [a,*], R.C. Belin [a], P.J. Valenza [a], A.C. Scheinost [b]

[a] CEA, DEN, DEC, CEN Cadarache F-13108 Saint-Paul-Lez-Durance, France
[b] Forschungszentrum Dresden-Rossendorf (FZD), Institute of Radiochemistry, P.O. Box 510119, 01314 Dresden, Germany

A B S T R A C T

The $^{241}Am_2Zr_2O_7$ phase undergoes a structural transition from pyrochlore to defect fluorite driven by alpha self-irradiation. In an effort to better understand the underlying phenomena of this order-disorder transition, powder X-ray diffraction (PXRD) and X-ray absorption fine-structure (XAFS) spectroscopy experiments were conducted on two samples aged for 40 days (0.02 dpa) and 370 days (0.21 dpa), respectively. While the XAFS data support the phase transition observed by XRD, they reveal different local coordinations of americium and zirconium. The transition occurs through oxygen Frenkel and cation antisite formation. The XAFS, clearly showed that the ZrO polyhedron is stable against irradiation, probably a main factor explaining the excellent resistance to amorphization observed for americium zirconia defect fluorite structures.

1. Introduction

Management of long-lived nuclear wastes is, after safety, the main issue of nuclear industry, both in terms of scientific challenge as well as public acceptance. Among the different options that have been envisioned and explored for minor actinides over the past 30 years, two alternatives currently remain: long term disposal in a safe repository or 'burning' of nuclear wastes in a so-called transmutation process. Materials selected for such applications have to meet the following criteria: high incorporation of actinides, good structural and chemical stability, low thermal dilatation and resistance to radiation.

The pyrochlore structure type $A_2^{3+}B_2^{4+}O_7$ is very attractive because of its ability to incorporate significant amounts of actinides. Radiation tolerance of titanate pyrochlore has been extensively studied either by ion irradiation or by incorporating short-lived actinide during synthesis (^{244}Cm or ^{238}Pu). All experimental results showed a systematic transition from crystalline to amorphous state [1–3]. Nevertheless, zirconate pyrochlores submitted to ion irradiation at very high doses (greater than 100 displacements per atoms) exhibit a phase transformation to a defect fluorite structure but remain crystalline [4,5].

However, in the prospect of transmutation and/or long term storage, this strong radiation tolerance has to be confirmed by experiments using materials doped with alpha-emitting minor actinides as in the case of nuclear glasses [6]. Due to the handling issues of highly radioactive elements, only limited studies are available [7,8]. Sykora et al. [9] reported the synthesis of $^{249}Cf_2Zr_2O_7$ pyrochlore and observed a phase transition into the defect fluorite structure after 6 months and a dose of 1.17×10^{18} α-decay events g^{-1}. In a previous study, $^{241}Am_2Zr_2O_7$ structure was described [10] and its evolution over a one year period followed by XRD [11]. The presence of 62 wt% of ^{241}Am ($t_{1/2}$ = 432 years) in the structure promoted fast aging due to α self-irradiation. The $^{241}Am_2Zr_2O_7$ sample evolved from the pyrochlore to a defect fluorite structure phase after ~370 days and remained unchanged afterwards. Thus, the resulting fluorite structure turns out to be resistant to self-irradiation within the time limit of the experiment.

Several experimental and theoretical studies were devoted to investigate the phase stability of the pyrochlore structure and its order–disorder transition to defect fluorite structure type [12,13]. Moreover, ion irradiation can also induce the formation of pyrochlore-fluorite intermediate structures [14].

X-ray absorption fine-structure (XAFS) spectroscopy with its ability to probe the local range (~6 Å) around a specific central atom and X-ray diffraction probing the long-range have been used as complementary techniques to study defective materials such as ion irradiated pyrochlores [15] or cubic stabilized Zirconia [16,17]. Consequently, to better understand the underlying phenomena involved in the order–disorder phase transition as well as the significant resistance to amorphization of the defect fluorite phase, we investigated the local environments of Am and Zr by XAFS.

2. Crystallography

The pyrochlore oxides of formula $A_2B_2O_6O'$ crystallize in the Fd-3m space group. Its structure is a superstructure based on the

* Corresponding author. Tel.: +33 4 42 25 38 66; fax: +33 4 42 25 32 85.
E-mail address: martinp@drncad.cea.fr (P.M. Martin).

0022-3115/$ - see front matter © 2008 Elsevier B.V. All rights reserved.
doi:10.1016/j.jnucmat.2008.10.028

fluorite-type structure like UO_2, except that there are two distinct crystallographic cation sites and 1/8th of the anions are absent. The atoms occupy the following special positions: A^{3+} at 16d, B^{4+} at 16c, O at 48f and O′ at 8b [18]. These positions are fixed by symmetry except the oxygen atom at the 48f position with unconstrained x parameter (x_{48f}). In the case of $Am_2Zr_2O_7$ the x_{48f} value is equal to 0.339 [10]. Furthermore, the 8a anion site, symmetrically identical to the 8b site, is empty. Thus, in the pyrochlore structure, the coordination shell of Am cations (8 oxygen atoms with 2 short Am–O′ distances and 6 longer Am–O) is distinct from that of Zr cations (6 equidistant O atoms), whereas the second coordination shell (cation–cation) is identical for both cations (6xAm + 6xZr at the same distance).

The structural phase transition from pyrochlore to defective fluorite involves the randomization of the oxygen anions among the 48f, 8b and 8a sites and of the cations between the 16c and the 16d sites. In the defect fluorite structure Am and Zr cations occupy the 4a crystallographic position while O anions are randomly occupying 7/8th of the 8c positions. Furthermore, an ideal fluorite structure type implies that the x_{48f} value is equal to 0.375. In such a structure, Am and Zr cations share the same position and thus have the same local environment: a first coordination shell consisting of 7 oxygen atoms at the same distance and the same second coordination shell as observed in the pyrochlore structure.

3. Experimental method

3.1. Sample preparation

The $Am_2Zr_2O_7$ starting material was prepared by mixing pure $^{241}AmO_2$ and ZrO_2 powders in the appropriate ratios followed by calcination at 1500 °C as previously described [10]. During the aging process, $^{241}Am_2Zr_2O_7$ powder was kept in a dry atmosphere without oxygen in order to prevent oxidation (pure N_2).

Two samples were shipped to the European Synchrotron Radiation Facility (ESRF): the first one was synthesised 40 days prior to the XAS experiment, the second a year before (370 days). Samples age corresponds to 0.02 dpa (2.7×10^{17} α-decay events g^{-1}) and 0.21 dpa (2.5×10^{18} α-decay events g^{-1}) respectively. The displacements per atom (dpa) were calculated using SRIM (The stopping and range of ions in matter) [19] with the commonly admitted value of 50 eV for displacement energy for all the atoms in the pyrochlore structure [12].

3.2. XRD data acquisition

Measurements were performed at room temperature with a Bragg–Brentano high resolution Siemens D5000 X-ray θ–2θ diffractometer using a curved quartz monochromator and copper radiation from a conventional tube source. Samples were mixed with epoxy resin and placed into a special in-house sample holder inside an inert atmosphere glove box to avoid oxidation [20]. X-ray powder diffraction patterns have been collected for as-synthesised, 40 day old (0.02 dpa) and 370 day old (0.21 dpa) samples. Data were refined by pattern matching using the JANA 2000 software [21].

3.3. EXAFS data acquisition and analysis

All XAS measurements were performed at the ESRF (Grenoble, France) at the Rossendorf beam line (BM20). Teflon sample holders were mounted in a closed-cycle He cryostat running at 15 K. For each sample, americium L_{II} (22952 eV) and zirconium K (17998 eV) edges spectra were collected in fluorescence mode using a 13 element Ge detector. The spectra were corrected for dead time using a measured relationship between incoming count rate (ICR) and selected channel analyzer (SCA) readings for each channel by using the SixPack software package. Energy calibrations were realized using a Y foil (17038 eV) or a Mo foil (20000 eV) positioned after the second ionisation chamber. The ATHENA software [22] was used for extracting XAFS oscillations from the raw absorption spectra. Experimental XAFS spectra were Fourier transformed using a Kaiser–Bessel window over the full k space range available for each edge: 2.1–13.3 $Å^{-1}$ for americium and 2.5–10.3 $Å^{-1}$ for zirconium. Curve fitting was performed in k^3 for R-values in the range 1.3–4.1 Å for both edges using calculated phases and amplitudes for the interatomic scattering paths using the *ab initio* code FEFF8.20 [23]. During curve fitting process attempts to introduce anharmonicity in the static disorder were performed by adding skewness in Am–O_{48f} or cation–cation distributions with a third cumulant [24]. As, no improvement of the fit and significant departure from values obtained without third cumulant were observed the anharmonicity hypothesis in our data was disregarded.

4. Results

4.1. XRD results

X-ray diffraction measurements performed prior to XAS measurements for the 0.02 dpa sample exhibit the pyrochlore structure with a cell parameter $a = 10.6686(1)$ Å. Compared to the 10.66849(4) Å of the as-synthesised [10], a small increase in cell parameter is observed. The 0.21 dpa sample showed the defect fluorite X-ray pattern with a cell parameter of $a = 5.3233(1)$ Å as superstructure peaks have vanished.

4.2. EXAFS results

4.2.1. Am environment

Am L_{II}-edge EXAFS spectra and their Fourier transforms are shown in Fig. 1 and fit results are given in Table 1. Considering the 0.02 dpa sample, the two Am–O distances present in the pyrochlore structure are observed with peaks at ~1.9 Å and ~2.2 Å. The low intensity of the second peak is due to 'the fact' that these two oxygen shell contributions interfere destructively which leads to relatively large uncertainty for Am–O distances (0.02 Å). The first distance (2.31(2) Å) represents the 8b oxygen atoms, the number of neighbours being slightly greater than expected (2.8(5) vs. 2.0). The second distance (2.53(2) Å) represents the 48f oxygen atoms. With 4.8(5) instead of 6.0, the number of neighbours is lower than expected. The fitted Am–O distance leads to a calculated value of 0.343 for the x_{48f} oxygen parameter. It is higher than the 0.339 value determined in the as-synthesised sample by Rietveld refinement [10]. Thus, disorder in the anionic sublattice is already observed for the 0.02 dpa sample, whereas, at first sight, the cationic sublattice is still identical as the two cation–cation distances are equal to the expected values.

Comparing 0.02 and 0.21 dpa samples on Fig. 1, evolution from the pyrochlore to the fluorite structure is quite evident. First of all, a systematic increase of Debye–Waller values in all coordination shells corroborates the expected increase of disorder. Next, the more intense first peak coupled with the fading peak at ~2.2 Å indicates that americium is surrounded by equidistant oxygen atoms. Shell fitting process confirmed this observation with 6.6(5) oxygen atoms at 2.35(1) Å. However, at the same time, the cation–cation shells included in the second peak at ~3.8 Å are clearly non-equivalent with 6.0(5) Am at 3.74(2) Å and 6.0(5) Zr at 3.65(2) Å. The order–disorder transition observed by XRD is confirmed but the observed structure appears more complex than expected.

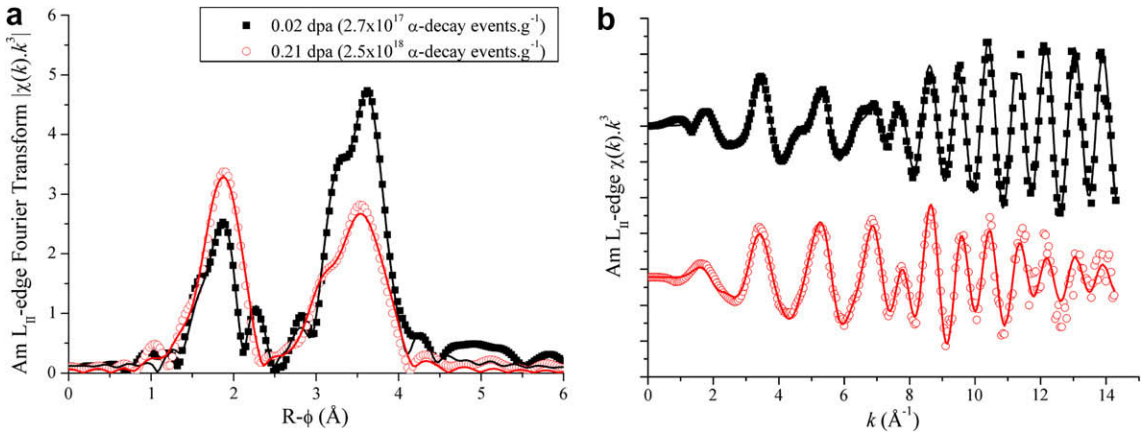

Fig. 1. Am L_{II}-edge EXAFS (b) and their Fourier transforms (a) for the 0.02 dpa and 0.21 dpa pyrochlore samples (experimental data are displayed by symbols and fit by lines).

Table 1
Am L_{II}-edge EXAFS fitting results for the two pyrochlore sample (the values in brackets are calculated interatomic distances in Å from XRD determination of lattice parameter).

Sample	0.02 dpa	0.21 dpa
Am–O_{8a}	[2.31]	[2.31]
Number	2.8(5)	6.6(5)
Distance (Å)	2.31(2)	2.35(1)
σ^2 (Å^2)	0.006(1)	0.009(1)
Am–O_{48f}	[2.565]	
Number	4.8(5)	X
Distance (Å)	2.53(2)	
σ^2 (Å^2)	0.015(1)	
Am–Am	[3.77]	[3.76]
Number	6.0(5)	6.0(5)
Distance (Å)	3.76(2)	3.75(2)
σ^2 (Å^2)	0.004(1)	0.007(1)
Am–Zr	[3.77]	[3.76]
Number	6.0(5)	6.3(5)
Distance (Å)	3.74(2)	3.65(2)
σ^2 (Å^2)	0.008(1)	0.012(1)
Am–O_{48f}	[4.32]	
Number	17(2)	X
Distance (Å)	4.26(4)	
σ^2 (Å^2)	0.01(1)	
R^2 (%)	0.9	0.9

Table 2
Zr K-edge EXAFS fitting results for the two pyrochlore sample (the values in brackets are calculated interatomic distances in Å from XRD determination of lattice parameter). Multi-scattering path values were linked to the corresponding single-scattering paths as described in the text.

Sample	0.02 dpa	0.21 dpa
Zr–O_{48f}	[2.11]	[2.31]
Number	6.3(5)	6.6(5)
Distance (Å)	2.13(2)	2.15(2)
σ^2 (Å^2)	0.005(1)	0.008(1)
Zr–Am	[3.77]	[3.76]
Number	6(1)	6(1)
Distance (Å)	3.75(2)	3.64(2)
σ^2 (Å^2)	0.004(1)	0.010(1)
Zr–Zr	[3.77]	[3.76]
Number	6(1)	6(1)
Distance (Å)	3.75(2)	3.51(2)
σ^2 (Å^2)	0.008(1)	0.017(1)
R^2	0.7	0.8

4.2.2. Zr environment

Zr K-edge EXAFS spectra and their Fourier transforms are shown in Fig. 2 and fit results given in Table 2. Note that the available fitting range is quite small due to the subsequent Am–L_{III} edge position. Furthermore, as suggested by FEFF calculation, a multi-

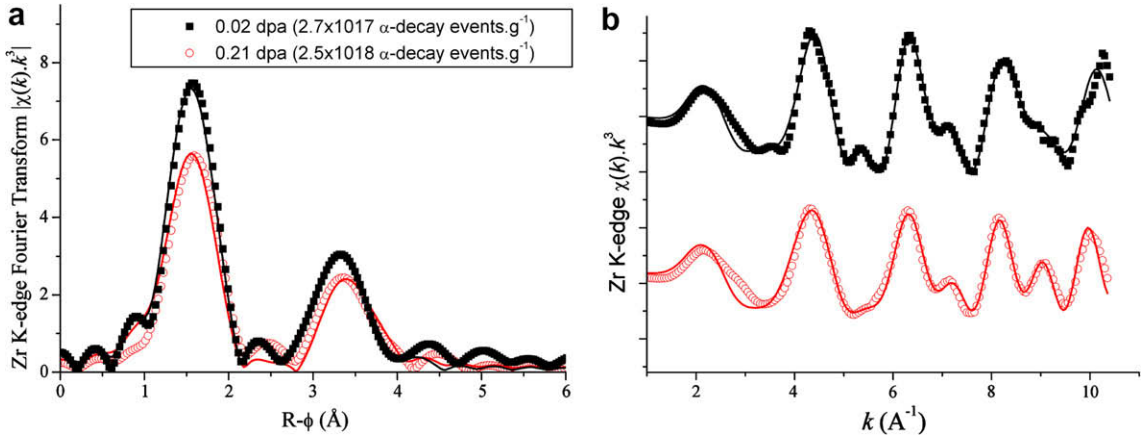

Fig. 2. Zr K-edge EXAFS (b) and their Fourier transforms (a) for the 0.02 dpa and 0.21 dpa pyrochlore samples (experimental data are displayed by symbols and fit by lines).

scattering path, corresponding to the doubling of the Zr–O single-scattering path (Zr–O–Zr–O), is required in the fitting process. Nevertheless, no extra parameters were introduced as the R and σ^2 were twice the values used for the Zr–O single-scattering shell.

Compared to the results for Am, aging had relatively little influence on the local structure around Zr as observed by Zr K-edge XAFS. Indeed, the transition from pyrochlore to defect fluorite-structure is not obvious with very few variations observed on the first coordination shell: 6.3(5) O at 2.13(1) Å for the 0.02 dpa sample and 6.6(5) O at 2.15(1) Å for the 0.21 dpa sample. The expected increase of both the number of neighbours and the Debye–Waller factors is observed, while bond distances remain nearly identical. This result is unexpected, as the pyrochlore to fluorite transformation should lead to a stronger difference. The, Zr–Am distances are very close to those observed at the Am L_{II}-edge and hence follow the predicted variation.

Evolution observed for Zr–Zr distances is more surprising. For the 0.02 dpa sample, the distance is equal to 3.75(2) Å in agreement with the pyrochlore structure. But considering the 0.21 dpa sample, the difference with values obtained from XRD data is quite evident with 3.51(2) Å instead of 3.77 Å. Clearly, the local environments of the Am and Zr cations follow a different evolution during order–disorder transition.

5. Discussion

Considering only XRD results and hence, only long-range order, we clearly observe a transformation from the pyrochlore into a defect fluorite structure and no amorphization.

In the $A_2Zr_2O_7$ pyrochlore structure, the A and B cation radii ratio are commonly used to estimate the stability of the pyrochlore structure against irradiation. For $Am_2Zr_2O_7$, using the 8-fold coordinated Am^{3+} radius value of 1.09 Å [25], this ratio ($r_A/r_B = 1.51$) is very similar to that of $Sm_2Zr_2O_7$, a stable pyrochlore compound exhibiting a phase transition to the defect fluorite structure when subjected to ion irradiation at 25 K [26]. The same behaviour occurs for $^{241}Am_2Zr_2O_7$ for a dose of 2.5×10^{18} α-decays events g^{-1} (0.21 dpa) and no amorphization is observed. Considering that $Sm_2Zr_2O_7$ remains crystalline for a very high dose corresponding to 7.3 dpa, this result was expected.

In the defect fluorite structure Am and Zr share the same crystallographic position implying an identical local environment. But, our EXAFS results provide a different picture as Am and Zr coordination shells are clearly non-equivalent.

The pyrochlore structure is unusual among oxides in that the order–disorder transition must occur in both the cation and anion sublattices. In the literature, different approaches have been considered to describe this transition: anionic disorder followed by cationic recombination [14], cationic disorder driving the transition [15] or concomitant occurrence of both cationic and anionic defects [4]. A more thorough study of the structural variations involved in the order–disorder transition should allow a better understanding of the $^{241}Am_2Zr_2O_7$ stability against alpha decay of americium.

First of all, considering the americium environment for the 0.02 dpa sample, an anionic disorder is clearly observed through a modified environment compared to the as-synthesised sample. This is in agreement with the oxygen Frenkel formation which consists of a vacancy on a 48f site and an interstitial on an 8a site, which is corroborated both by the increase of the x_{48f} parameter and by the lower number of oxygen 48f neighbours. The occurrence of cationic disorder is not obvious as previously discussed. But, the number of O 8b neighbours observed around Am (2.8(5) atoms at 2.31(2) Å) contradicts the space group symmetry imposing only 2 atoms. These two evidences confirm an Am^{3+} and Zr^{4+} exchange (cation antisite formation) in the 0.02 dpa sample as proposed by atomistic calculations [13].

However, no apparent anionic disorder is observed around Zr and the Zr–O distance of 2.13(1) Å is in agreement with the respective ionic radii. This seems to indicate that ZrO polyhedra are still identical to that of the as-synthesised sample. However, the Zr–Zr Debye–Waller factor value (0.008(1) $Å^2$) is significantly higher compared to Zr–Am (0.004(1) $Å^2$). As proposed by previous studies [27,15], disorder could be accommodated by rotations of the ZrO polyhedra across corners and shared-edges. This hypothesis can be asserted by studying the environment observed on the 0.21 dpa sample where the order–disorder transition is complete, involving total randomization of oxygen between the free sites and an inversion of the cations. In the 0.21 dpa sample, Am and Zr are both 7-fold coordinated, which is in agreement with the 7/8th oxygen occupancy factor of the defect fluorite structure. However, zirconium forms a more compact polyhedron (2.15(1) Å vs. 2.35 Å.). This Zr–O distance is identical to the value observed by Li et al. [28] in Fe and Ga-doped monoclinic zirconia with 7-fold coordinated zirconium.

The difference between Am and Zr local environments can be explained as there is substantial evidence, from both experiment and computation, that the oxygen vacancy, rather than being nearest neighbour to Am, has a strong tendency to associate with Zr, rendering the tetravalent cation 7-coordinate, as in the monoclinic phase of ZrO_2 [29].

The XAFS studies on doped zirconia by Li et al. [16] showed that for oversized trivalent dopants such as yttria, the created oxygen vacancies are located as nearest neighbours of Zr. The location of the vacancies leads to the existence of ZrO_7 polyhedra which are not regular features of the fluorite-type. Such behaviour implies a strong distortion of the Zr cation shell. A similar distortion is observed in the 0.21 dpa sample (decreased of Zr–Zr distance), corroborating our assumption that the structure is able to accommodate disorder through ZrO polyhedra across corners and shared-edges.

Zacate et al. [30] have used atomistic calculations on trivalent doped zirconia systems. They conclude that systems with oversized dopants (e.g. Am^{3+}) will be energetically more stable when oxygen vacancies are gathered near zirconium.

6. Conclusion

XAFS spectroscopy, through its capacity to explore the local order around specific elements, proved to be a useful technique to complement X-ray diffraction [31,32]. We were able to follow the order–disorder transition induced by alpha decay in the $Am_2Zr_2O_7$ phase. Our study shows that the disorder occurs on both anionic and cationic sublattices through oxygen Frenkel and cation antisite formation. Thank to EXAFS, we observed different local environments for americium and zirconium cations. The transition appears to be rather a disruption of the long-range order probed by XRD. Our work, coupled with other studies on trivalent-doped zirconia, demonstrate that the ZrO polyhedron is very stable. This stability is most likely one of the key factors explaining the good resistance to amorphization observed for americium zirconia defect fluorite structures.

References

[1] J. Lian, L. Wang, J. Chena, K. Sun, R.C. Ewing, J.M. Farmer, L.A. Boatner, Acta Mater. 51 (2003) 1493.
[2] W.J. Weber, J.W. Wald, Mater. Lett. 3 (1985) 173.
[3] J. Lian, J. Chen, L.M. Wang, R.C. Ewing, J.M. Farmer, L.A. Boatner, K.B. Helean, Phys. Rev. B 68 (2003) 134107.
[4] K.E. Sickafus, L. Minervini, R.W. Grimes, J.A. Valdez, M. Ishimaru, F. Li, K.J. Mc Clellan, T. Hartmann, Science 289 (2000) 748.

[5] S.X. Wang, B.D. Begg, L.M. Wang, R.C. Ewing, W.J. Weber, K.V.G. Kutty, J. Mater. Res. 14 (1999) 4470.
[6] W.J. Weber, R.C. Ewing, C.A. Angell, G.W. Arnold, A.N. Cormack, J.M. Delaye, D.L. Griscom, L.W. Hobbs, A. Navrotsky, D.L. Price, A.M. Stoneham, M.C. Weinberg, J. Mater. Res. 12 (1997) 1946.
[7] G.R. Lumpkin, R.C. Ewing, Phys. Chem. Miner. 16 (1988) 2.
[8] W.J. Weber, J.W. Wald, Hj. Matzke, J. Nucl. Mater. 138 (1986) 196.
[9] R.E. Sykora, P.E. Raison, R.G. Haire, J. Solid State Chem. 178 (2005) 578.
[10] R.C. Belin, P.J. Valenza, P.E. Raison, M. Tillard, J. Alloys Compd. 448 (2008) 321.
[11] R.C. Belin et al., Actinides 2005 Conference – Recent Advances in Actinide Science 4–8 July, University of Manchester RSC Publishing, Manchester (UK), 2005.
[12] R.C. Ewing, W.J. Weber, J. Lian, J. Appl. Phys. 95 (2004) 5949.
[13] L. Minervini, R.W. Grimes, K.E. Sickafus, J. Am. Ceram. Soc. 83 (2000) 1873.
[14] J. Lian, W.J. Weber, W. Jiang, L.M. Wang, L.A. Boatner, R.C. Ewing, Nucl. Instrum. and Meth. B 250 (2006) 128.
[15] N.J. Hess, B.D. Begg, S.D. Conradson, D.E. McCready, P.L. Gassman, W.J. Weber, J. Phys. Chem. B 106 (2002) 4663.
[16] P. Li, I.W. Chen, J.E. Penner-Hahn, Phys. Rev. B 48 (1993) 10074.
[17] C.R.A. Catlow, A.V. Chadwick, G.N. Greaves, L.M. Moroney, J. Am. Ceram. Soc. 69 (1986) 272.
[18] M.A. Subramanian, G. Aravamudan, G.V. Subba Rao, Prog. Solid State Chem. 15 (1983) 55.
[19] J.F. Ziegler, J.P. Biersack, U. Littmark, The Stopping and Range of Ions in Solids, Pergamon, New York, 1985.
[20] R.C. Belin, P.J. Valenza, M.A. Reynaud, P.E. Raison, J. Appl. Cryst. 37 (2004) 1034.
[21] V. Petricek, M. Dusek, L. Palatinus, JANA 2000. The Crystallographic Computing System, Institute of Physics, Praha, Czech Republic, 2000.
[22] B. Ravel, M. Newville, J. Syn. Rad. 12 (2005) 537.
[23] J.J. Rehr, R.C. Albers, Rev. Mod. Phys. 72 (2000) 621.
[24] D.C. Koningsberger, R. Prins, X-ray Absorption: Principles, Applications Techniques of EXAFS, SEXAFS, and XANES, Wiley, New York, 1988.
[25] R.D. Shannon, Acta Cryst. A 32 (1976) 751.
[26] J. Lian, X.T. Zu, K.V.G. Kutty, J. Chen, L.M. Wang, R.C. Ewing, Phys. Rev. B 66 (2002) 054108.
[27] R.C. Ewing, B.C. Chakoumakos, G.R. Lumpkin, T. Murakami, R.B. Greegor, F.W. Lytle, Nucl. Instrum. and Meth. B 32 (1988) 487.
[28] P. Li, I.W. Chen, J. Am. Ceram. Soc. 77 (1994) 118.
[29] A. Navrotsky, J. Am. Chem. 15 (2005) 1883.
[30] M.O. Zacate, L.M. Minervini, D.J. Bradfield, R.W. Grimes, K.E. Sickafus, Solid State Ionics 128 (2000) 243.
[31] F.J. Espinosa-Faller, R.C. Howell, A.J. Garcia-Adeva, S.D. Conradson, A.Y. Ignatov, T.A. Tyson, R.F.C. Farrow, M.F.J. Toney, Phys. Chem. B 109 (2005) 10406.
[32] R.C. Howell, S.D. Conradson, A.J. Garcia-Adeva, J. Phys. Chem. B 111 (2007) 159.